Lightweight Self-Forming Super-Elastic ~~Mechanical Meta-materials~~ with Adaptive Stiffness

Rui Wu Peter C.E. Roberts Shida Lyu Fei Zheng Constantinos Soutis Carl Diver Dekai Zhou Longqiu Li* Zongquan Deng*

Dr. R. Wu, Dr. P. C. E. Roberts, Dr. S. Lyu, Prof. C. Soutis
The University of Manchester Aerospace Research Institute, Manchester, M13 9PL, UK.
Email Address: wurui_hit@hit.edu.cn
Dr. F. Zheng
School of Materials, The University of Manchester, Manchester, M13 9PL, UK.
Dr. C. Diver
The Manchester Metropolitan University, Manchester, M15 6BH, UK.
Dr. R. Wu, Dr. D. Zhou, Prof. L. Li, Prof. Z. Deng
Laboratory of Robotics and System, Harbin Institute of Technology, Harbin, 150001, P. R. China
Email Address: longqiuli@hit.edu.cn

Keywords: *architectured material, pseudoelasticity, active material, self-stressing*

Scarcity of stiff, yet compliant materials is a major obstacle toward biological-like mechanical systems that perform precise manipulations while being resilient under excessive load. We introduce a macroscopic cellular structure comprising of two pre-stressed elastic "phases", which displays a load-sensitive stiffness that drops by 30 times upon a "pseudo-ductile transformation" and accommodates a fully-recoverable compression of over 60%. This provides an exceptional 20 times more deform-ability beyond the linear-elastic regime, doubling the capability of previously reported super-elastic materials. In virtue of the pre-stressing process based on thermal-shrinkage, it simultaneously enables a heat-activated self-formation that transforms a flat laminate into the metamaterial with 50 times volumetric growth. The metamaterial is thereby inherently lightweight with a bulk density in the order of 0.01 g cm^{-3}, which is one order of magnitude lower than existing super-elastic materials. Besides the highly-programmable geometrical and mechanical characteristics, this paper is the first to present a method that generates single-crystal or poly-crystal-like 3D lattices with anisotropic or isotropic super-elasticity. This pre-stress-induced adaptive stiffness with high deform-ability could be a step toward in-situ deployed ultra-lightweight mechanical systems with a diverse range of applications that benefit from being stiff and compliant.

1 Introduction

Flexible mechanical systems, including soft robotics, wearable devices and compliant mechanisms have attracted tremendous research interest in the recent years. However, mimicking the ability of living organisms to maintain geometrical stability for precise manipulations while being resilient to tolerate shock and allow shape transformations remains a challenge due to the intrinsic limitation of materials [1, 2]: high-modulus materials such as metallic alloys and ceramics only allow small elastic strain before permanent deformation or fracture, whilst highly-resilient materials such as hyper-elastic elastomers suffer from low rigidity. Although natural super-elastic shape memory materials offer a variable modulus arising from stress-induced microscopic phase transformations (Figure S1b in the Supporting Information), it is dedicated to only a small group of crystalline materials that suffer from insufficient strain capacity ($<$10%), high material density (5$\sim$10 g cm^{-3}) and narrow operating temperature window [3–6]. However, recent studies in soft robotics are beginning to tackle this trade-off [1, 2], with new horizons opened up by the introduction of mechanical metamaterials where macroscopic modular structures made from conventional materials are assembled to achieve extreme and programmable mechanical properties that are not found in naturally occurring materials [7–10].

In the field of mechanical metamaterials it has been shown that cellular structures can shift from high modulus to highly compliant under a certain external load through controlled ligament buckling, which transforms the high-modulus pre-buckling scenario to the bending-dominated post-buckling scenario with low-incremental-stiffness "pseudo-ductile" response (Figure S1c in the Supporting Information). The metamaterial designs include: elastomers with arrays of voids that buckle under compression by a broken rotational symmetry [11–15]; interlinked curved compliant beams with snap-through buckling [16,17]; micro-lattices that accommodate partially-recoverable deformation through shell buckling [18, 19]. However, tuning of buckling requires these cellular structures to have bulky ligaments with a reasonably low slenderness ratio, which fundamentally limits the deform-ability and lightweightness, restricting their fully-recoverable deformation to $<$30% and bulk density to 0.2$\sim$1 g cm^{-3}.

Here we report a fundamentally different approach to achieve a self-adapting stiff-to-compliant transformation, together with high deform-ability, low bulk density and in-situ self-formation. Based on this approach we created a mechanical metamaterial comprising of two elastic "phases" pre-loaded against each other. Upon a certain external load, its stiffness drops by 30 times and a fully-recoverable compression of $>$60% is achieved, expanding the deformation envelope by 20 times beyond linear elasticity. Motivated by the recent progress in self-formation that converts 2D sheets into intricate 3D objects using kirigami [20–25], origami [26–28] and layered structures [29–33], the metamaterial has also achieved remotely controlled in-situ deployment. When heated, it transforms from a thin laminate into 3D configurations with approximately 50 times volumetric growth, leading to a low bulk density in the range of 0.02$\sim$0.05 g cm^{-3}. In comparison with the buckling-induced super-elasticity, it has doubled the deformation-enhancing-ability while reducing the bulk density by one order of magnitude. Meanwhile, the overall geometry and mechanical response can be programmed by tailoring the design parameters and the arrangement of structural cells. Utilizing Voronoi patterns, we demonstrated a method that generates single/poly-crystal-like 3D lattices with anisotropic/isotropic super-elasticity.

2 Results and Discussion

2.1 Design of the Super-Elastic Metamaterial

As illustrated in **Figure 1**, the metamaterial is fabricated as a stack of flat "constrainers" (polyester heat-shrinking film, "Mylar HS") and "deformers" (thermally-stable polyimide film, "Kapton") selectively bonded by adhesive (pressure-sensitive acrylic adhesive from the "3M 966 adhesive transfer tape"). When heated, the thermal-shrinkage of the "constrainers" induce pre-stress into the stack, transforming it into pre-stressed unit cells. The metamaterial expands by approximately 50 times during this process and transform from a flexible thin laminate into the 3D volumetric configuration (Figure 1b). This creates a scenario where two elastic "phases", i.e. the resilient "deformer" and high-modulus tension-only "constrainer" are pre-loaded against each other, which gives rise to the stiffness adaptation.

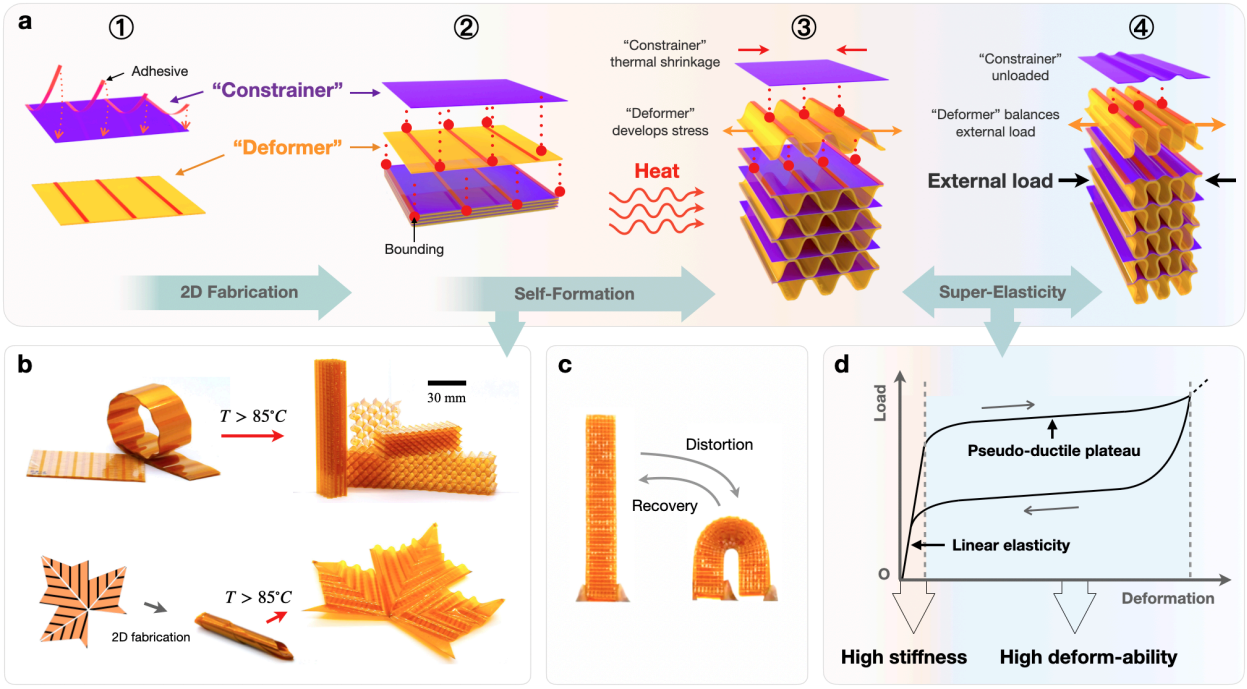

Figure 1. Super-elastic mechanical metamaterial with heat-activated self-formation. (a) From a stack of "constrainer" and "deformer" films bounded at selected sites, the metamaterial forms under the thermal shrinkage of "constrainer", which pre-load the "deformer" to create a 50-times volumetric expansion and accommodate large deformation. (b) Test samples transform from flexible thin laminates into volumetric materials. (c) The metamaterial accommodates significant distortion and fully recovers upon unloading. (d) The pre-stress within the metamaterial induces super-elasticity with a load-sensitive stiffness adaptation: once a critical load is reached, the mechanical response departs from linear-elastic with its stiffness dramatically reduced and undergoes a "pseudo-ductile" behavior, allowing it to be rigid, yet highly-deformable.

Under an increasing compression, the high-modulus "phase" dominates the mechanical response until the pre-stress is fully released under external load and the resilient "phase" takes over. The metamaterial thereby switches from high-modulus to a low-incremental-modulus "pseudo-ductile" scenario upon a certain external load determined by the level of pre-stress, as further discussed in Section 2.3. Such process is reversible during unloading as far as the constituent material remains in the elastic region. This pre-stressed design allows the metamaterial to be constructed solely from thin-films, leading to a high porosity when formed, which is the key to achieving lightweightness and deformation accommodation. The highly-programmable geometry and mechanical response are further demonstrated in Section 2.4.

2.2 Mechanical Characteristics of the Metamaterial

Stiffness-adaptation provided by super-elasticity significantly expands the material performance envelope, which allows high-modulus structures to be loaded beyond the linear-elastic limit and deformed in a resilient manner, and enables flexible structures to bear considerable initial load with low deflection thus high precision. The key to achieving an outstanding performance is to stretch the strain envelop beyond linear-elasticity as far as possible. Therefore, we define a figure of merit Φ to characterize the degree of super-elasticity as the ratio between the maximum allowable deformation (strain) ϵ_{max} and the critical deformation at "pseudo-ductile" yielding ϵ_{cr}: $\Phi = \epsilon_{max}/\epsilon_{cr}$. Systematic comparison between different types of super-elastic materials is then carried out, as shown in **Figure 2**e where the figure of merit is plotted against bulk density. It can be seen that the conventional super-elastic crystalline materials including metallic alloys and Zirconia ceramic (at small scale) only achieves mild super-elastic characteristics (in terms of Φ) according to literature [6]. The existing mechanical metamaterials that obtain super-elasticity from instability-induced pattern transformations, including elastic solids with 2D [11, 12, 14] or 3D voids [15], and 2D curved beams [16] are one order of magnitude lighter than conventional systems, but exhibit similar degree of super-elasticity. For the proposed metamaterial, the figure of merit Φ is evaluated with $\epsilon_{cr} = 0.03$ and $\epsilon_{max} = 0.6$ according to compression tests (Figure 2d). This gives a Φ value of 20, which doubles the best existing metamaterial's performance and triples the Ni-Ti alloy's performance. One $\sim$ two orders of magnitude reduction in bulk density is also achieved.

Such striking performance is a result of the pre-stressed design: unlike the instability-induced super-elasticity that requires relatively bulky structural elements for instability-tuning, the tension-only "constrainer" and the resilient "defomer" in the pre-stressed cellular metamaterial can be constructed using high-performance thin-film materials. This allows a significantly higher porosity, and thereby lower bulk density and more space to accommodate deformation.

Arrays of unit cells can be assembled into a 3D volumetric metamaterial, which displays two modes of typical "pseudo-ductile" deformation: unidirectional compression along the shrink-

age direction and bending perpendicular to the Mylar layers (Figure 2d, and Movie S2 in the Supporting Information). Such macroscopic behaviors can be predicted by integrating the local compressive responses of the unit cells (details included in the Supporting Information). According to the compression test, the incremental compressive modulus between 0% $\sim$ 3% compression (linear-elastic region) and 10% $\sim$ 30% compression ("pseudo-ductile" plateau) are 36 kPa and 1.3 kPa respectively. For bending, the incremental rigidity between 0 mm $\sim$ 1 mm deflection (with a support span of 90 mm) and 5 mm $\sim$ 30 mm deflection are 1.21 N mm^{-1} and 0.0375 N mm^{-1} respectively. The super-elastic metamaterial therefore provides two distinct operating modes switched upon the "pseudo-ductile transformation", with its modulus varied by approximately 30 times. Meanwhile, it can be seen in Figure 2b that the unit cells bifurcate into a slightly tilted shape, which leads to a near-zero Poissons ratio during the pseudo-ductile compression. This bifurcation minimizes bending within the sandwiched sections of the laminate and thereby minimizes strain energy, as further discussed in Supporting Information.

2.3 Mechanism of the Pre-Stress-Induced Super-Elasticity

During pre-stressing, the Kapton films are elastically loaded against the Mylar and form a shape similar to wave-springs, thereby create a scenario where resilient "deformers" are pre-loaded by high-modulus tension-only "constrainers". Figure 2f (and Figure S1d in the Supporting Information) provides an intuitive illustration of such a system, which is an equivalent model where the "deformers" and "constrainers" are represented by two springs loaded in parallel with the stiffness of k_1 and k_2, respectively. Super-elasticity requires that $k_1 \ll k_2$ and k_2 to be effective only in tension. Under initial state after self-formation, equilibrium requires the loads from the "deformer", $F_{def} = k_1\epsilon_1$ and the "constrainer", $F_{con} = k_2\epsilon_2$ to satisfy $F_{def} = F_{con}$, where ϵ stands for deformation (strain). Thus super-elasticity requires $\epsilon_2 \ll \epsilon_1$. For the test samples we have $\epsilon_1 = 0.35$ according to the thermal-shrinkage mismatch between the "deformers" and the "constrainers", and $\epsilon_2 = 0.03$ according to compression test results. With a small compression $\Delta\epsilon$ developed under an external compressive force F_{ext}, the equilibrium becomes:

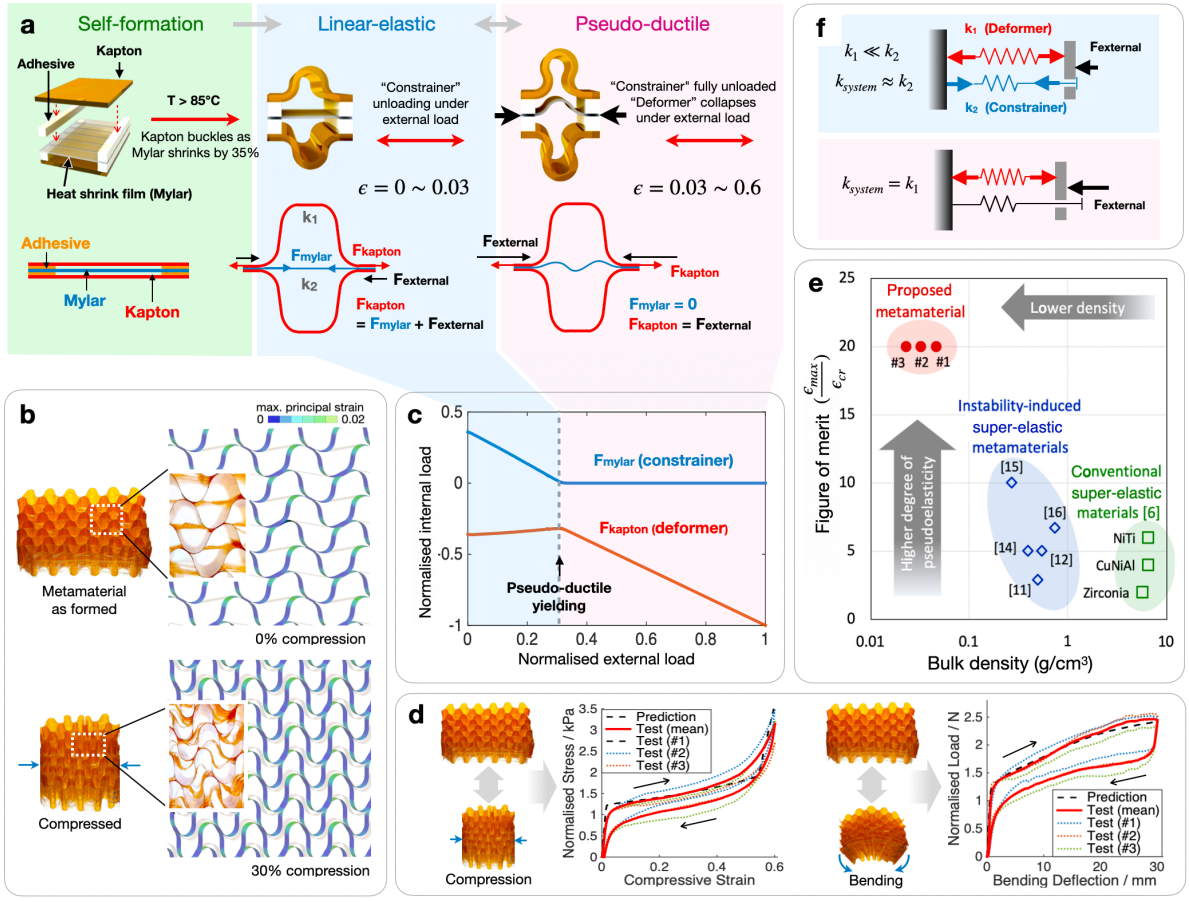

Figure 2. Mechanical metamaterial with pre-stress-induced super-elasticity. (a) Unit cell forms and obtains super-elasticity utilizing the pre-stressing induced by thermal-shrinkage. (b) Experimental and computational results on the evolution of geometrical characteristics during compression. (c) Simulation reveals that the super-elasticity originates from the transfer of stress between "constrainer" and "deformer". (d) Experimental and computational results of super-elastic response during compression and bending. (e) Systematic comparison with existing materials indicating remarkable improvement in super-elasticity and lightweightness achieved by this study. (f) Equivalent parallel-spring model of a unit cell.

$$F_{ext} - F_{def} + F_{con} = F_{ext} - k_1(\epsilon_1 + \Delta\epsilon) + k_2(\epsilon_2 - \Delta\epsilon) = 0 \quad (\Delta\epsilon \leq \epsilon_2) \tag{1}$$

As far as the "constrainers" are still under tension, the effective stiffness of the system is: $k_{linear} = dF_{ext}/d\epsilon = k_1 + k_2 \approx k_2$. Then at the critical deformation $\epsilon_{cr} = \epsilon_2$, the "constrainers" are fully unloaded and have no resistance to compression ($F_{con} = 0$), the equilibrium becomes:

$$F_{ext} - F_{def} = F_{ext} - k_1(\epsilon_1 + \Delta\epsilon) = 0 \quad (\Delta\epsilon > \epsilon_2) \tag{2}$$

Thus the system stiffness becomes $k_{yield} = k_1$. This marks the beginning of the "pseudo-ductile" plateau, which continues until the deformer is fully collapsed at $\epsilon_{max} > \epsilon_1 \gg \epsilon_{cr}$. The metamaterial thereby has a high figure of merit ($\epsilon_{max}/\epsilon_{cr}$), and a significant drop in incremental-stiffness upon "pseudo-ductile" yielding since $k_{yield} \ll k_{linear}$. The discussion above agrees with the Finite Element (FE) simulation results shown in Figure 2c (details included in the Supporting Information). It is worth noting that such a super-elastic mechanism is somehow similar to the phase-transformation in super-elastic shape memory alloys, which also shift behavior under a critical load by releasing strain energy contained in one phase and achieve yielding with low incremental stiffness through a reversible lattice-distortion process (Figure S1 in the Supporting Information). Therefore, similar to shape memory alloys, such a super-elastic response is repeatable as far as the pre-stressed scenario is maintained.

2.4 Programming the Mechanical and Geometrical Features

2.4.1 Scalability of the Unit Cell

The effect of scaling can be illustrated using the classical model for 2D cellular structures with linear elastic material behavior. This introduces an effective stiffness, S proportional to the cube of ligament slenderness ratio [34]: $S \propto (t/l)^3$, where t is the cell ligament thickness and l is the characteristic length of the unit cell. For the samples used in this study, t is set to be 25 μm according to the thickness of Kapton, and l is set to the cell span (definition of cell span can be found in Figure S7e in the Supporting Information), which are 7 mm, 10 mm and 14 mm for the three sample sets #1, #2 and #3, respectively. Therefore, a normalized stress Q can be expressed as below (using the dimensions of design #2), which stays independent of cell size as far as geometrical similarity is maintained and the same film materials are used:

$$Q = \sigma \cdot \left(400 \cdot \frac{t}{l}\right)^{-3} \tag{3}$$

The average values of the normalized compressive stress and bending load measured from the three sets of samples are reported in Figure 2d. More information can be found in Figure S7 in the Supporting Information, where the simulation results on mechanical response and deformed shapes show satisfactory agreement with experiment. Meanwhile, Equation 3 also suggests that the overall compression resistance of the metamaterial increases with deformer membrane thickness and modulus, as well as reducing cell span. Such result indicates that the mechanical properties of the metamaterial can be programmed for specific applications, and this pre-stressed metamaterial design can adapt to wide range of scales.

2.4.2 Interconnected Unit Cells Along Linear Paths

It is demonstrated in Figure 2b that a 3D volumetric metamaterial can be constructed by joining the unit cells together along straight linear paths. Here it is shown that besides the basic rectangular configuration shown before, the overall geometry of the metamaterial can be designed by tailoring the shape of unit cells and the curvature of linear path. This allows the metamaterial to form various geometries and achieve design-able mechanical properties. Three examples are provided below in **Figure 3** to demonstrate such design-ability.

The annular-shaped metamaterial shown in Figure 3a is formed from an annular laminate where regular unit cells are distributed along a circular path, and shrinkage occurs along the tangential direction. Since the total shrinkage along any concentric path is equal, the resulted structure is a circular ring with a uniform shrinkage in diameter (from 110 mm to 90 mm). The super-elastic behavior when compressed along the diameter allows it to be used as a soft wheel that maintains low deflection thus low resistance to rolling, while tolerating over-load conditions. The structure in Figure 3b is formed using an annulus-sector-shaped laminate similar to the one discussed above, but with conical unit cells. The tangential shrinkage thereby varies linearly along radius, thus the beam curvature changes during heat activation. As the conical cells are formed,

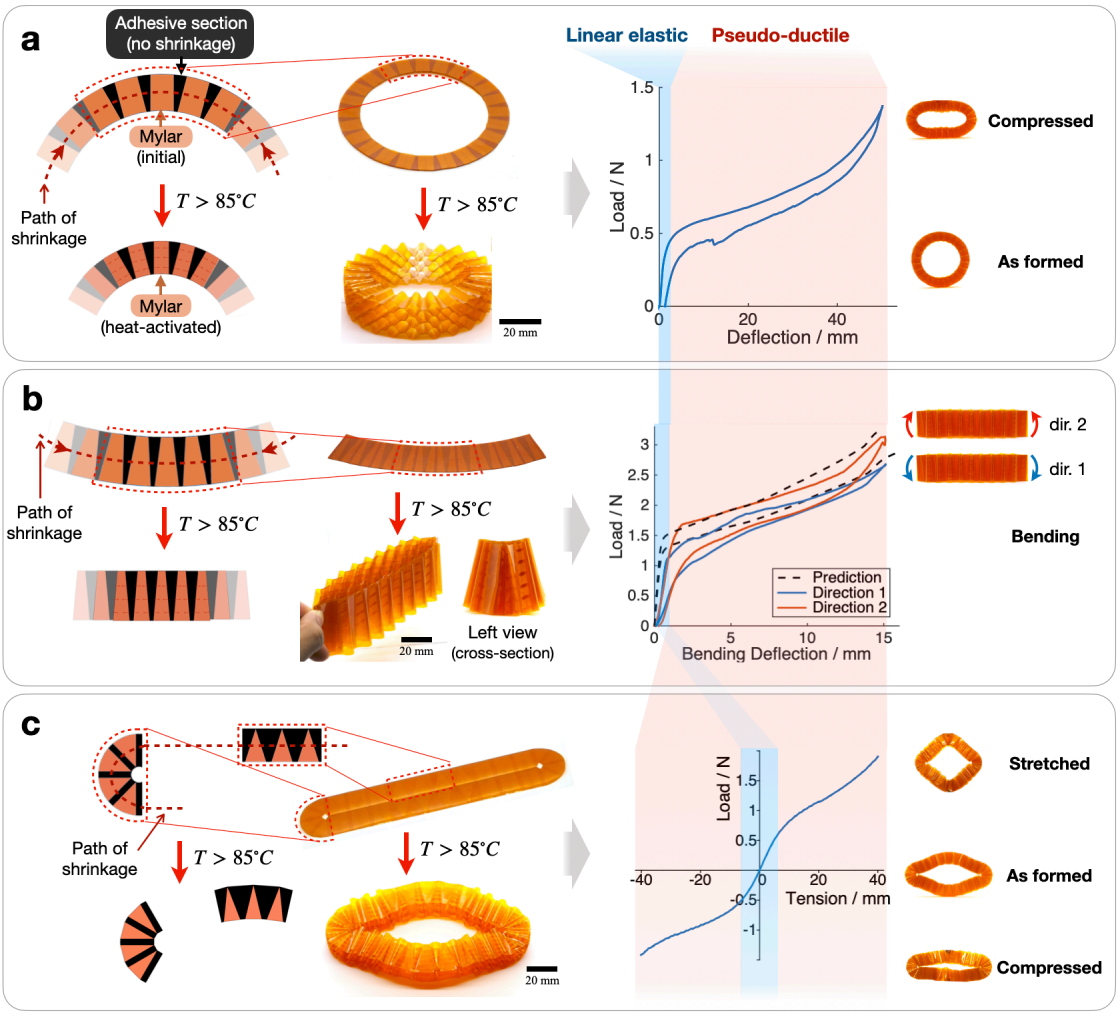

Figure 3. Metamaterials with tailored shapes based on unit cells interconnected along linear paths. (a) Annular structure based on regular cells distributed along a circular path exhibits super-elasticity when compressed along the diameter. (b) Bi-stiffness beam with conical cells distributed along a circular path displays different bending rigidity along two directions. (c) Diamond-shaped frame based on various types of unit cells displays super-elasticity in both compression and tension.

the structure transforms into a straight beam with trapezoidal cross-section. The conical unit cells lead to bi-stiffness behavior: since the cells near the wider (lower) edge of the trapezoid have larger size and thus lower stiffness (Equation 3), the bending along the direction which results in compression in the larger cells (i.e. direction 1 as illustrated in the figure) displays lower rigidity. Simulation model (detailed in Supporting Information) and 3-point bending tests have verified such bi-stiffness characteristics (Figure 3b). The diamond-shaped super-elastic frame

shown in Figure 3c is based on a combination of different unit cells discussed above. The frame undergoes bending deformation when subject to normal load as illustrated in the figure, providing super-elastic response in both compression and tension.

2.4.3 Interconnected Unit Cells Along Voronoi Patterns

All the super-elastic structures discussed above are based on unit cells distributed along linear paths, i.e. the principal directions of thermal shrinkage. Although the versatility in mechanical behavior can be enhanced utilizing the super-elastic bending response, as demonstrated in Figure 3c, the linear cell arrangement still limits the compressive super-elastic response to only one principal direction, i.e. along the shrinkage direction. However, when the unit cells are distributed along a more complex 2D pattern, e.g. a Voronoi diagram, a 3D lattice of inter-connected unit cells can be created under a uniform planar shrinkage, which provide compressive super-elastic response along any directions within the plane of shrinkage (**Figure 4**). The reason to chose a Voronoi diagram is that such a pattern allows the plane of shrinkage to remain planar during cells formation (see Supporting Information).

Geometry of Voronoi patterns depend on the distribution of seeds upon which the diagram is constructed. The pattern is thereby inherently programmable. As shown in Figure 4a and b, the metamaterial design starts from a 2D hexagonal distribution of seeds, upon which the Voronoi diagram is plotted, which is then used to determine the edges of the unit cells. Samples are constructed using the same method as illustrated in Figure 1, while self-formation is induced using heat-shrinking films with isotropic thermal shrinkage. The result is a super-elastic lattice consisted of regular unit cells interconnected along a hexagonal pattern, which exhibits an anisotropic super-elastic response when compressed along the plane of thermal shrinkage. Such a highly-ordered structure with anisotropic modulus is similar to single crystals. By tailoring the Voronoi pattern, an isotropic, polycrystalline behavior is also achievable.

Voronoi diagrams are often used to resemble the grain domains of polycrystalline materials, thereby inherently allow the design of an isotropic lattice [35, 36]. As shown in Figure 4c and d, a metamaterial with in-plane near-isotropic response is designed based on a Voronoi pattern

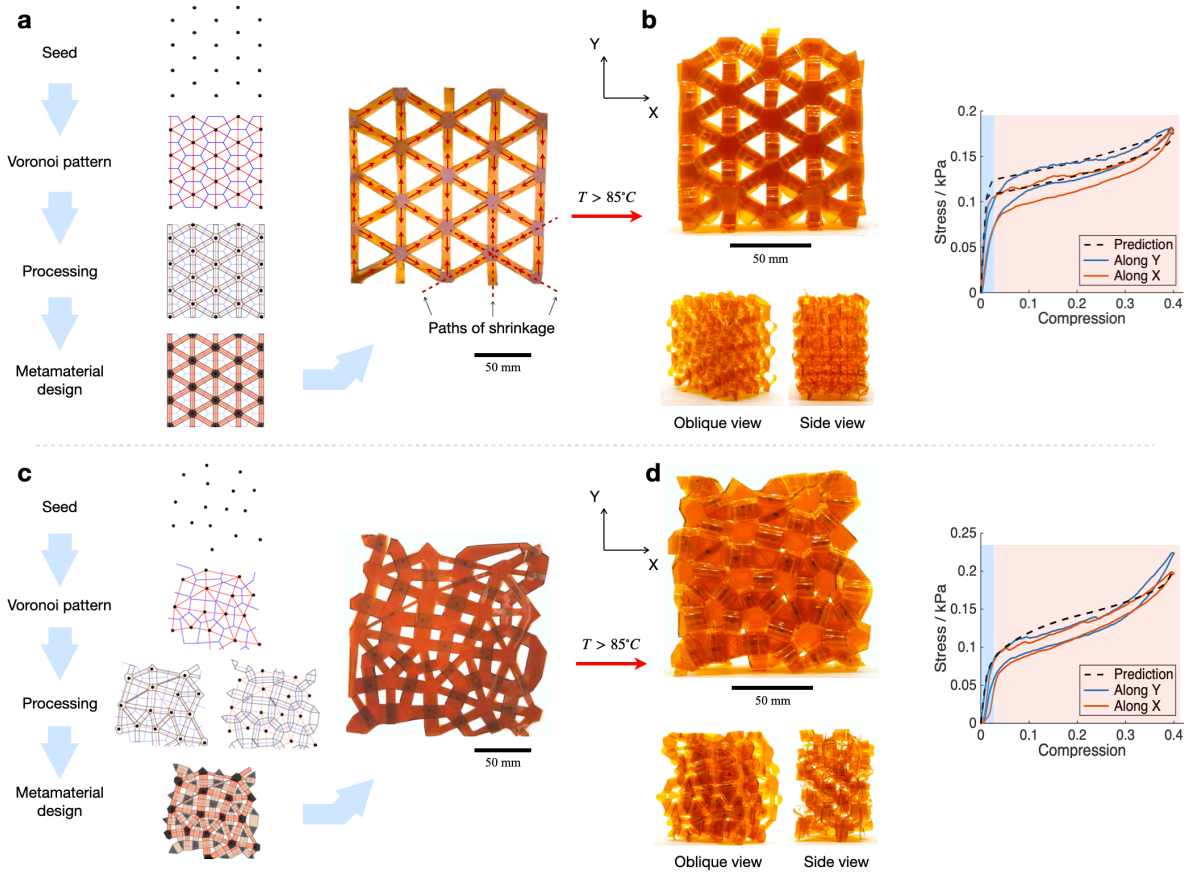

Figure 4. Single/poly-crystal-like metamaterials with anisotropic and isotropic in-plane super-elasticity, based on unit cells interconnected along Voronoi patterns (see Supporting Information). (a) Laminate designed from a 2D distribution of seeds in a hexagonal pattern. (b) 3D single-crystal-like hexagonal lattice formed through an uniform in-plane shrinkage, which exhibits anisotropic super-elasticity when compressed along any directions within the plane of shrinkage. (c) Laminate designed from a random 2D distribution of seeds. (d) 3D polycrystal-like lattice formed through an uniform in-plane shrinkage, which exhibits near-isotropic super-elasticity when compressed along any directions within the plane of shrinkage.

constructed upon randomly distributed seeds. To enhance isotropy, two different cell patterns with geometrical correlation are derived from the same Voronoi diagram (Figure 4c), and used to create two types of laminates that are alternatingly stacked together to form the metamaterial (see Supporting Information). The resulted metamaterial exhibits isotropic mechanical response similar to an equiaxes polycrystalline material (Figure 4d). This provides a method to automatically generate isotropic super-elastic 3D lattices at any scales.

2.5 Demonstration of Super-Elastic Metamaterials

The adaptive-stiffness super-elastic behavior enables soft robots that carry load in a high-stiffness manner while being compliant to allow shape morphing and tolerate shock. The super-elastic whisker shown in **Figure 5**a – c is installed on the edge of a thin-film force sensor, which output a non-zero force signal when the whisker is touched to enable tactile sensing. Enabled by the high-stiffness response, it achieves high sensitivity by producing high output under low deflection, whilst the "pseudo-ductile" response enables an intrinsic over-load protection that maintains acceptable pressure on the film sensor while tolerating significant distortion and strikes. Another example is illustrated in Figure 5d – e, where a robotic gripper utilizes the high-modulus linear-elastic response of the super-elastic fingers to pick up small objects with a considerable gripping force, whilst the "pseudo-ductile" response allows gripping of significantly larger objects with unknown shape. The stiffness-adaptation provides a near-constant gripping force to guarantee effective gripping of objects across a wide range of sizes without overloading (Figure 5f).

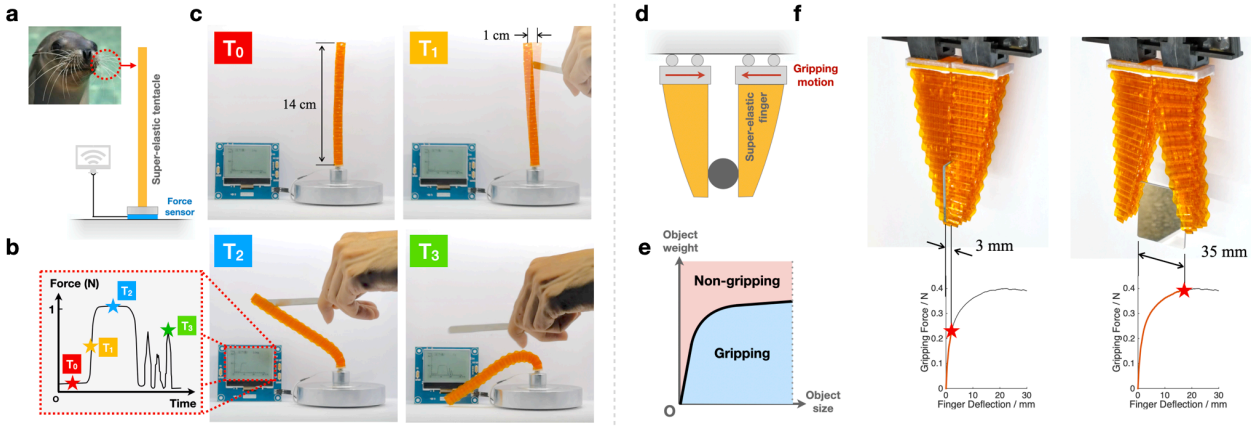

Figure 5. Potential applications in super-elastic soft robots. (a) Super-elastic whisker mounted above a thin film pressure sensor that outputs force signal when the whisker is distorted. (b and c) The device achieves high sensitivity at low deflection while tolerating large distortion and strikes, thanks to its super-elastic response. (d and e) Versatile soft gripper with pseudoelastic fingers, where stiffness-adaptation enables constant gripping force at a wide range of finger deflections, allowing effective gripping of small and large objects, as demonstrated by (f) gripping of a piece of glass along its thickness and width.

Figure 6 demonstrates the application as a super-elastic building material, which harnesses

its lightweightness, in-situ deployment, and the ability to carry load in a high-stiffness manner while repeatably tolerating high deformation without notable mechanical degradation. As an example, the model of an in-situ self-constructed emergency shelter remains sturdy and secure under normal loading scenario, while tolerating significantly higher load and rapidly recovers after extreme crushing (Figure 6b, Movie S3 in the Supporting Information). The super-elastic characteristic also makes it robust against strong wind: unlike trees in the nature that sways elastically before fracturing at a wind speed of around 40 m s^{-1} [37], the shelter behaves like a rigid structure with little deformation at a wind speed under 30 m s^{-1}, and after exposed to stronger wind, it immediately returns to upright with no structural damage (Figure 6c). During strong wind, the shelter sways by pseudo-ductile deformation, which reduces the drag area thus limits the wind load while maintaining a safe space inside. In addition, the lightweight flat package and self-formation with little human intervene also lead to low storage profile and transportation/installation cost. These features are ideal for buildings installed in a harsh environment with scarcity of resources and limited capacity of transportation, such as for emergency deployment or planetary explorations.

3 Conclusion

It has been shown that a cellular material system comprising of elastically distorted "deformers" and pre-loaded "constrainers" displays strong super-elasticity with an adaptive stiffness that drops by 30 times upon a certain external load. As a result, it exhibits a counter-intuitive behavior that shifts from high modulus to highly compliant under a certain external load. Meanwhile, the pre-loading process based on a heat-activated shrinkage simultaneously enables self-formation that transforms a flat multi-layered laminate into the volumetric metamaterial while expanding its volume by approximately 50 times, leading to an inherently lightweight configuration with a bulk density in the order of 0.01 g/cm^3, which is at least one order of magnitude lower than existing super-elastic materials. While retaining the high-stiffness linear-elastic response that occurs below 3% compression, super-elasticity significantly enlarges its operational deformation to over 60%.

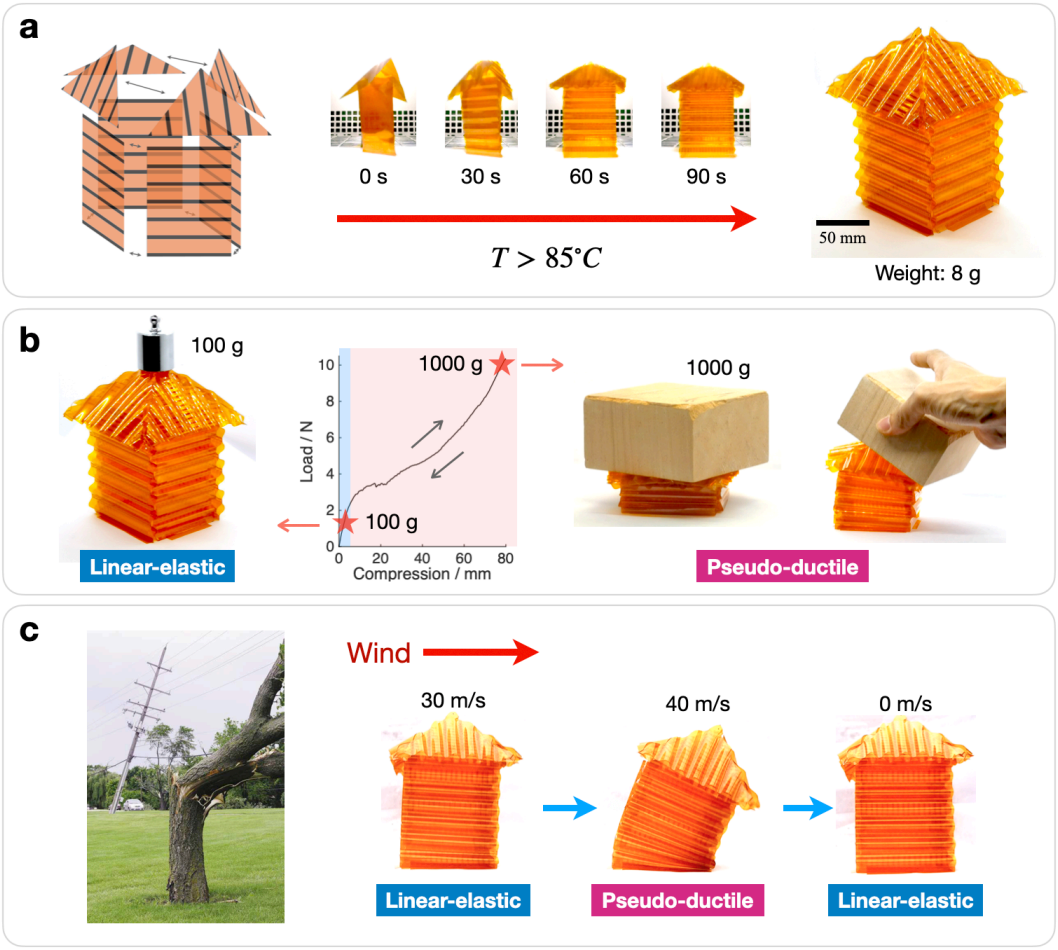

Figure 6. Demonstration of super-elastic building material for rapid deployment in harsh environment. (a) Model of a super-elastic emergency shelter self-constructed from a flat-package through heat-activation in an oven. (b) The 8 g model supports a 100 g of load in a high-stiffness manner while recovers after being crushed under a 1 kg load, thanks to super-elasticity. (c) Unlike trees in the nature that sways and fractures at high wind, the model behaves as a rigid shelter at wind speed under 30 m s^{-1}, but sways resiliently under stronger wind and immediately returns to upright as wind reduces (photo: Ken Schulze).

Such a 20-times-improvement of deformation envelop has doubled the performance of existing super-elastic materials, as characterized by the figure of merit (Φ). The metamaterial has also demonstrated programmable mechanical response and overall geometry. Automatic method to design 3D super-elastic lattices with single-crystalline, anisotropic or polycrystalline, isotropic characteristics is created by arranging unit cells along 2D Voronoi patterns. In summary, the present study provides a unique method to realize strong super-elastic characteristics, and a

versatile framework to enable in-situ deployed adaptive-stiffness mechanical metamaterials that are inherently lightweight and programmable. These properties can be harnessed to realize future advanced mechanical systems at a wide range of scales, including soft robots, wearable devices, medical stents, mechanical energy dissipators, and self-deploying space structures.

4 Experimental Section

Sample fabrication::

The metamaterial is fabricated using membrane materials including: "Kapton HN" polyimide film manufactured by "Dupont" with a thickness of 25.4 μm; "Mylar HS" polyester heat shrink film manufactured by "Dupont" with a thickness of 16 μm; "3M acrylic adhesive transfer tape 966" with a thickness of 50 μm. Samples are fabricated by laminating layers of 2D precursors cut into the desired 2D patterns using a CNC vinyl cutter (Figure S8 in the Supporting Information). Alignment and stacking of the 2D precursors are conducted manually using a customized tool. In order to reduce the unwanted local stress in the formed unit cell, the Mylar is cut into strips to make the shrinkage along the width of the strips less-constrained thus relax under thermal-activation. This converts the near-isotropic shrinkage to unidirectional along the length of the strips, and significantly reduces the residual stress within the adhesive layer. During layup, coatings of primer is applied onto the surface of Kapton and Mylar to enhance their adhesion to the acrylic adhesive. Heat-activation is conducted at approximately 95°C (above the glass transition temperature of 85°C) under air convection using an oven.

Mechanical testing::

All mechanical tests are conducted using a standard Instron machine with a 50 N or 20 N load cell, at a crosshead speed of 1 mm s^{-1}. Customized test fixtures are used in compression tests to eliminate the boundary effects and guarantee uniform deformation, so that the samples behave as within an infinitely-large body of metamaterial under unidirectional compression (Figure S6 in the Supporting Information). The test fixtures are designed to eliminate the effect of friction from the boundary constrainers, the details of which is further discussed in the Supporting Information.

Finite Element Analysis (FEA) of a pre-stressed unit cell::

Nonlinear 2D FE analysis are carried out in ANSYS to predict the mechanical response and geometrical transformation of a unit cell. The simulation uses a Representative Volume Element (RVE) that represents half of a unit cell within an infinitely-large body of the metamaterial (Figure S2 in the Supporting Information). Due to the small thickness of the membrane materials, the maximum strain of Kapton material is always below 2% during self-formation and compression, thus the materials are treated as linear elastic isotropic for simplicity. The material properties are acquired from the official datasheet: Kapton has a Young's modulus of 2.76 GPa, and a Poisson's ratio of 0.34; Mylar has a Young's modulus of 3.1 GPa, and a Poisson ratio of 0.4; acrylic adhesive has a thickness of 50 μm and is assumed to be rigid (the sections with adhesive have no visible bending deformation during experiments, thus are treated as rigid by constraining all the local deformations, for the sake of computational efficiency). The simulation begins from the flat laminate configuration, and the buckling-induced self-formation is simulated by applying a 35% thermal shrinkage to Mylar. Buckling direction is determined by applying a small biased force, which reduces to zero before the end of self-formation. The resulted geometry is then further deformed to reveal the mechanical response of a unit cell under unidirectional compression.

Prediction of the macroscopic behaviors::

The unit cells distort uniformly under macroscopic compression, thus the overall resistance to compression is simply proportional to the number of cells loaded in parallel. Under bending, the distortion of each cell varies linearly through the thickness of the metamaterial whilst the degree of distortion depends on the local bending moment. This allows the metamaterial behavior to be predicted using unit cells compressive response retrieved from FE simulations. The details can be found in the Supporting Information.

Supporting Information

Supporting Information is available from the Wiley Online Library or from the author.

Acknowledgements

This research was partially supported by the National Natural Science Foundation of China

(51822503), and the State Key Laboratory of Robotics and System (SKLRS201813B). R.W. acknowledges support from the University of Manchester School of Mechanical Aerospace and Civil Engineering, the University of Manchester Aerospace Research Institute, the Cookson Memorial Fund supported by Professor Henry Wright Baker in support of the postgraduate research project, and the Postdoctoral International Exchange Program of China for the postdoctoral fellowship.

References

[1] Y. Tang, Y. Chi, J. Sun, T.-H. Huang, O. H. Maghsoudi, A. Spence, J. Zhao, H. Su, J. Yin, *Sci. Adv.* **2020**, *6*, 19 eaaz6912.

[2] S. Mintchev, J. Shintake, D. Floreano, *Sci. Robot.* **2018**, *3*, 20 eaau0275.

[3] J. M. Jani, M. Leary, A. Subic, M. A. Gibson, *Mater. Des.* **2014**, *56* 1078.

[4] K. Otsuka, C. Wayman, *Mechanism of shape memory effect and superelasticity*, Cambridge University Press, Cambridge, UK, **1998**.

[5] F. Auriemma, C. De Rosa, S. Esposito, G. R. Mitchell, *Angew. Chem. Int. Ed. Engl.* **2007**, *119*, 23 4403.

[6] A. Lai, Z. Du, C. L. Gan, C. A. Schuh, *Science* **2013**, *341*, 6153 1505.

[7] V. Hahn, P. Kiefer, T. Frenzel, J. Qu, E. Blasco, C. Barner-Kowollik, M. Wegener, *Adv. Funct. Mater.* **2020**, 1907795.

[8] H. Li, M. Rosendo-López, Y. Zhu, X. Fan, D. Torrent, B. Liang, J. Cheng, J. Christensen, et al., *Research* **2019**, *2019* 8345683.

[9] K. Bertoldi, V. Vitelli, J. Christensen, M. van Hecke, *Nat. Rev. Mater.* **2017**, *2*, 11 17066.

[10] K. H. Lee, K. Yu, A. Xin, Z. Feng, Q. Wang, et al., *Research* **2020**, *2020*.

[11] T. Mullin, S. Deschanel, K. Bertoldi, M. C. Boyce, *Phys. Rev. Lett.* **2007**, *99*, 8 084301.

[12] K. Bertoldi, P. M. Reis, S. Willshaw, T. Mullin, *Adv. Mater.* **2010**, *22*, 3 361.

[13] B. Florijn, C. Coulais, M. van Hecke, *Phys. Rev. Lett.* **2014**, *113*, 17 175503.

[14] S. Willshaw, T. Mullin, *Soft Matter* **2012**, *8*, 6 1747.

[15] S. Babaee, J. Shim, J. C. Weaver, E. R. Chen, N. Patel, K. Bertoldi, *Adv. Mater.* **2013**, *25*, 36 5044.

[16] A. Rafsanjani, A. Akbarzadeh, D. Pasini, *Adv. Mater.* **2015**, *27*, 39 5931.

[17] K. Che, C. Yuan, J. Wu, H. J. Qi, J. Meaud, *J. Appl. Mech.* **2017**, *84*, 1 011004.

[18] X. Zhang, J. Yao, B. Liu, J. Yan, L. Lu, Y. Li, H. Gao, X. Li, *Nano Lett.* **2018**.

[19] L. R. Meza, S. Das, J. R. Greer, *Science* **2014**, *345*, 6202 1322.

[20] N. An, A. G. Domel, J. Zhou, A. Rafsanjani, K. Bertoldi, *Adv. Funct. Mater.* **2020**, *30*, 6 1906711.

[21] X. Ning, X. Wang, Y. Zhang, X. Yu, D. Choi, N. Zheng, D. S. Kim, Y. Huang, Y. Zhang, J. A. Rogers, *Adv. Mater. Interfaces* **2018**, *5*, 13 1800284.

[22] T. C. Shyu, P. F. Damasceno, P. M. Dodd, A. Lamoureux, L. Xu, M. Shlian, M. Shtein, S. C. Glotzer, N. A. Kotov, *Nat. Mater.* **2015**, *14*, 8 785.

[23] Y. Tang, G. Lin, S. Yang, Y. K. Yi, R. D. Kamien, J. Yin, *Adv. Mater.* **2017**, *29*, 10 1604262.

[24] A. Rafsanjani, K. Bertoldi, *Phys. Rev. Lett.* **2017**, *118*, 8 084301.

[25] W. Wang, C. Li, H. Rodrigue, F. Yuan, M.-W. Han, M. Cho, S.-H. Ahn, *Adv. Funct. Mater.* **2017**, *27*, 7 1604214.

[26] J. Cui, J. Adams, Y. Zhu, *Smart Mater. Struct.* **2017**, *26*, 12 125011.

[27] J. Cui, F. R. Poblete, Y. Zhu, *Adv. Funct. Mater.* **2018**, 1802768.

[28] Y. Chen, R. Peng, Z. You, *Science* **2015**, *349*, 6246 396.

[29] D.-Y. Khang, H. Jiang, Y. Huang, J. A. Rogers, *Science* **2006**, *311*, 5758 208.

[30] S. Xu, Z. Yan, K.-I. Jang, W. Huang, H. Fu, J. Kim, Z. Wei, M. Flavin, J. McCracken, R. Wang, et al., *Science* **2015**, *347*, 6218 154.

[31] Y. Zhang, Z. Yan, K. Nan, D. Xiao, Y. Liu, H. Luan, H. Fu, X. Wang, Q. Yang, J. Wang, et al., *Proc. Natl. Acad. Sci.* **2015**, *112*, 38 11757.

[32] Z. Yan, F. Zhang, J. Wang, F. Liu, X. Guo, K. Nan, Q. Lin, M. Gao, D. Xiao, Y. Shi, et al., *Adv. Funct. Mater.* **2016**, *26*, 16 2629.

[33] Z. Yan, F. Zhang, F. Liu, M. Han, D. Ou, Y. Liu, Q. Lin, X. Guo, H. Fu, Z. Xie, et al., *Sci. Adv.* **2016**, *2*, 9 e1601014.

[34] L. J. Gibson, *J. Biomech.* **2005**, *38*, 3 377.

[35] K. Kobayashi, K. Sugihara, *Future Gener. Com. Sy.* **2002**, *18*, 5 681.

[36] D. Goswami, S. Liu, A. Pal, L. G. Silva, R. V. Martinez, *Adv. Funct. Mater.* **2019**, *29*, 24 1808713.

[37] E. Virot, A. Ponomarenko, É. Dehandschoewercker, D. Quéré, C. Clanet, *Phys. Rev. E* **2016**, *93*, 2 023001.